Dataset: A turbulent bluff-body stabilised H_2-flame

Eirik Æsøy, James R. Dawson

Department of Energy and Process Engineering, Norwegian University of Science and Technology, Trondheim N-7491, Norway

1. Description

This document provides a description of a dataset taken of a turbulent bluff body stabilised hydrogen flame in the single flame combustor at NTNU in Trondheim. The flame was produced by a lean fully premixed air/hydrogen mixture and was stabilized in the recirculation zone produced by a conical bluff body. The flame was unconfined and the ambient conditions in terms of temperature and pressure were 1 atm and 25 °C. Flames and flow produced by the same geometry have been investigated extensively in the following list of references featuring the same flame holder geometry and covering similar blends and velocities as the ones provided in this dataset [1, 2, 3, 4, 5, 6, 7, 8].

This dataset contains measurements of the non-reacting and reacting velocity flow fields as well as intensity from OH-Chemiluminecence and OH-PLIF, taken at the bluff body center plane. Both time series data and statistics in terms of mean and r.m.s. fields are provided. If you have any queries, please contact one of the corresponding authors through the contact details at the bottom of this page.

1.1. Geometry

A schematic of the burner geometry is shown in figure 1. A computer-aided drawing (CAD) of the geometry is provided in the CAD folder as "Geometry.step" and "Geometry.STL" files. A cut of the sections is displayed in figure 1(a). For a more in-depth description of the facility see [5]. Premixed gas enters through two opposing jets (labeled Gas inlets) into the bottom of a plenum section. The mixture is then expanded for flow conditioning before being contracted into an injector pipe with an inner diameter of $d_p = 19\,\text{mm}$ as shown in figure 1(b). At the end of the injector pipe, labeled the "dump plane", the flow expands into the room. At the center of the pipe, a flame holder consisting of a bluff body with a diameter of $d_b = 13\,\text{mm}$ and an inclination angle of 45°, is held by a 5 mm rod. The purpose of the bluff body is to generate a resirculation zone where the flame can stabilise in the shear layers. To center the rod/bluff body in the pipe, a set of 2 mm cylinders was placed at a distance 65 mm upstream of the dump plane. As such, the rod is held in place at the bottom of the pipe and supported by these cylinders. As discussed in [2, 3, 7], upstream geometry like these can potentially influence flame dynamics. Hence, these were made smaller and placed sufficiently far upstream ($> 35D$) to reduce their significance as compared to previous studies. The Cartesian coordinate system $x - y - x$ is centered at the bluff body with directions as indicated in figure 1.

The materials used for the different rig parts and their thermal properties are summarised in table 1. The injector pipe, bluff body/rod, dump plane plate, and base plate were made out of stainless steel. These are labeled "Injector parts" in figure 1(a). The components in the plenum section were made out of aluminum. These are labeled "Plenum parts" in figure 1(a).

Email addresses: eirik.asoy@ntnu.no (Eirik Æsøy), james.r.dawson@ntnu.no (James R. Dawson)

Table 1: Table of materials and material properties.

Material	K (W/mK)	α (1/K)	Components
Stainless steel (AISI 347)	16.3	$1.7e-5$	Injector parts
Aluminium (1060 Alloy)	230	$2.3e-5$	Plenum parts

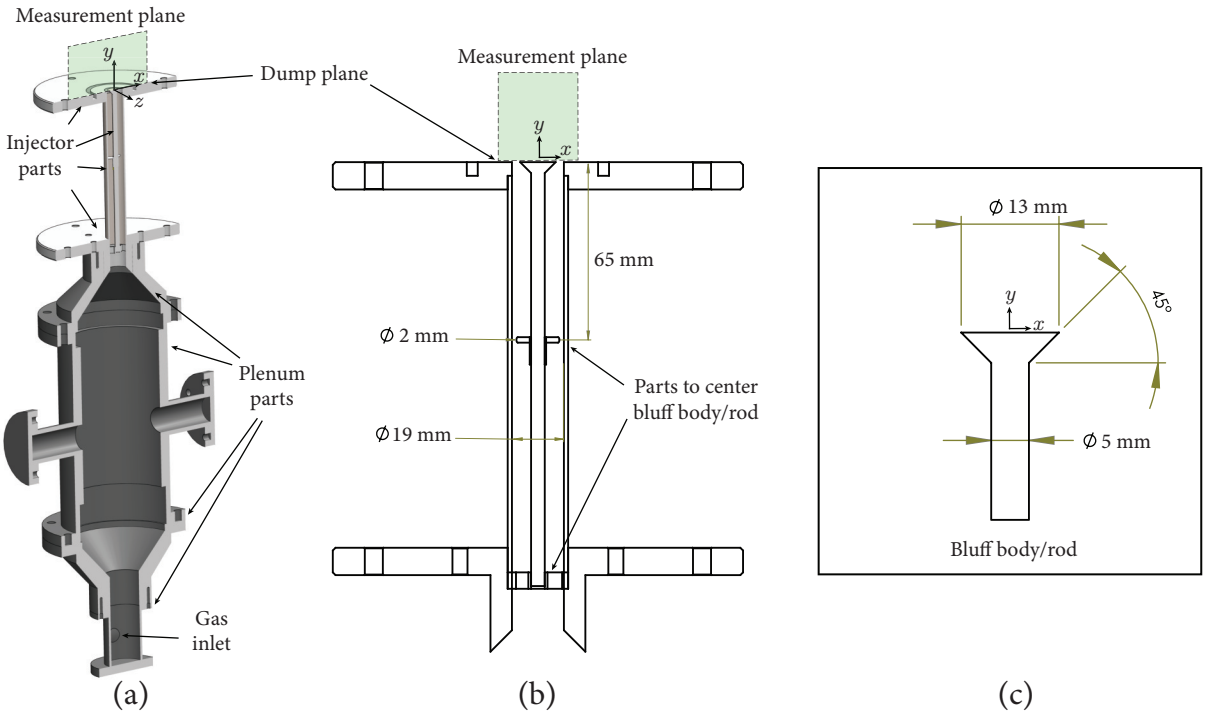

Figure 1: (a) Schematic of the single sector combustor. (b) Schematic of the injector pipe assembly. (c) Schematic of the bluff body/rod.

Case	P (kW)	$\bar{u}$ (m/s)	Φ	$\dot{Q}_{\text{air}}$ (m^3/s)	$\dot{Q}_{\text{H}_2}$ (m^3/s)	$\dot{m}_{\text{air}}$ (g/s)	$\dot{m}_{\text{H}_2}$ (g/s)	T_{in} (°C)	T_{s} (°C)
1	3.5	15	0.4	19.33×10^{-4}	3.25×10^{-4}	2.258	0.0292	25	25

Table 2: Operating conditions: P is the thermal power, $\bar{u}$ the nozzle bulk velocity, the equivalence ratios Φ, and flow rates $\dot{Q}_{\text{air}}$ and $\dot{Q}_{\text{H}_2}$ of air and hydrogen. T_{in} and T_{s} are the temperatures of the gas mixture and surroundings.

1.2. Operating conditions

The database consists of one operating condition and the parameters are summarised in Table. 2. The goal was to have a "simple" flow and geometry. The inlet mixture temperature and the ambient temperature were both room temperature at T_{In} and $T_{\text{s}} = 25°$.

	$E_{\dot{Q}}$ (MJ/m^3)	$E_{\dot{m}}$ (MJ/kg)
H_2	10.8	120

Table 3: Gas properties in terms of the energy per unit volume $E_{\dot{Q}}$ and energy per unit mass $E_{\dot{m}}$.

A brief summary of how the flow and fuel quantities are defined is provided below. The gas properties in terms the lower heating values for air and hydrogen are summarised in table 3. From

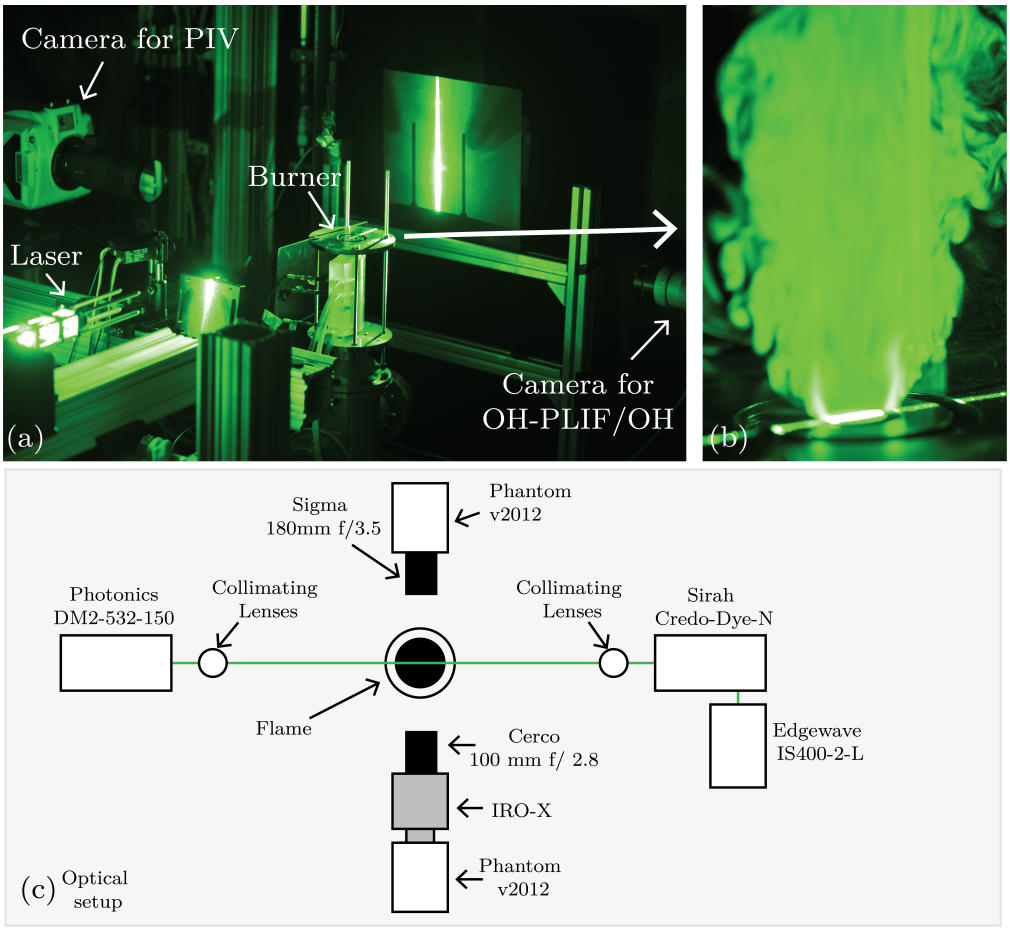

Figure 2: (a) Picture of the setup showing the two cameras used for PIV and OH-PLIF/OH Chemiluminescence. (b) Picture of the flame. (c) Schematic of the optical set-up.

these and the flow rates, the thermal power is given by

$$P = \dot{Q}_{\mathrm{H_2}} E_{\dot{Q}} = \dot{m}_{\mathrm{H_2}} E_{\dot{m}} = 3.5\,\mathrm{kW} \tag{1}$$

where $E_{\dot{Q}}$ and $E_{\dot{m}}$ are the lower heating value per unit volume and mass.

The bulk velocity $\bar{u}$ at the dump plane is obtained by dividing the total volume flow rate by the nozzle exit area

$$\bar{u} = \frac{Q_{\mathrm{air}} + Q_{\mathrm{H_2}}}{A_e} = \bar{u} = 15\,\mathrm{m/s}, \tag{2}$$

where $A_e = 0.25\pi(d_p^2 - d_b^2)$ is the nozzle exit area.

The equivalence ratio (ratio of molecules of fuel and oxidiser, relative to stoichiometric conditions) is given by

$$\Phi = \frac{0.5\dot{Q}_{\mathrm{H_2}}}{0.21\dot{Q}_{\mathrm{air}}} = 0.4, \tag{3}$$

where the factor 0.21 is the volume fraction of oxygen in the air where $\dot{Q}_{\mathrm{O_2}} = 0.21\dot{Q}_{\mathrm{air}}$.

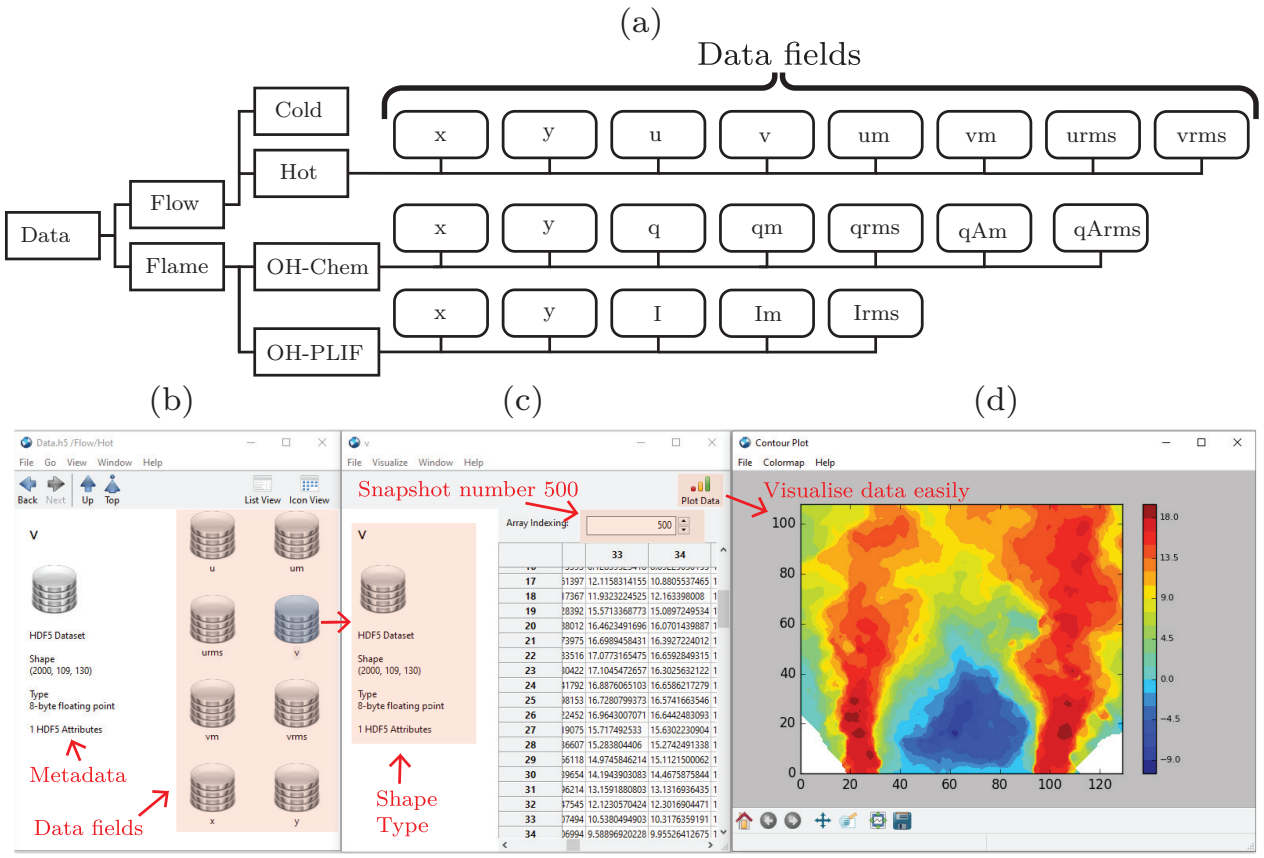

Figure 3: HDF5 files structure. This file can easily be opened and visualized by using a HDF viewer software, e.g. "HDF compass". (a) Schematic of the hierarchical structure. (b) File opened using "HDF compass". (c) Data field from the Flow → Hot → "v". (d) Data field v visualized.

2. Measurements

In this section, the measured quantities are described. A picture of the diagnostic setup is shown in figure 2(a) and (b). The optical set-up is shown schematically in (c). A two-camera setup using two Phantom V2012 1 Mpx cameras combined with planar laser diagnostics was used to obtain:

1. **Flow velocity:** Two components of the velocity field (u, v) in the centre $x - y$ plane.
2. **OH-chemiluminescence:** An estimate of the HRR from OH-chemiluminescence.
3. **OH-PLIF:** Intensity from OH-PLIF in the centre $x - y$ plane.

For all fields, a number of 2000 instantaneous fields as well as statistics in terms of time-averaged and r.m.s. fluctuation fields are provided. A description of each of the fields and how they are organized is as follows.

The data fields are stored in an HDF5 file format and the file is named "Data.h5". The hierarchical structure of the file is shown in figure 3(a). All data fields are stored as a matrix of float (8-byte). The fields consist of n_x by n_y spatial sampling points and n_t temporal points. For the fields containing time series data, e.g. u and v, the sampling rate is stored as Metadata. The file structure can easily be accessed and browsed by using a HDF viewer software, such as "HDF compass" which is open source and runs on any operating system. An example is shown in figure 3(b-d),

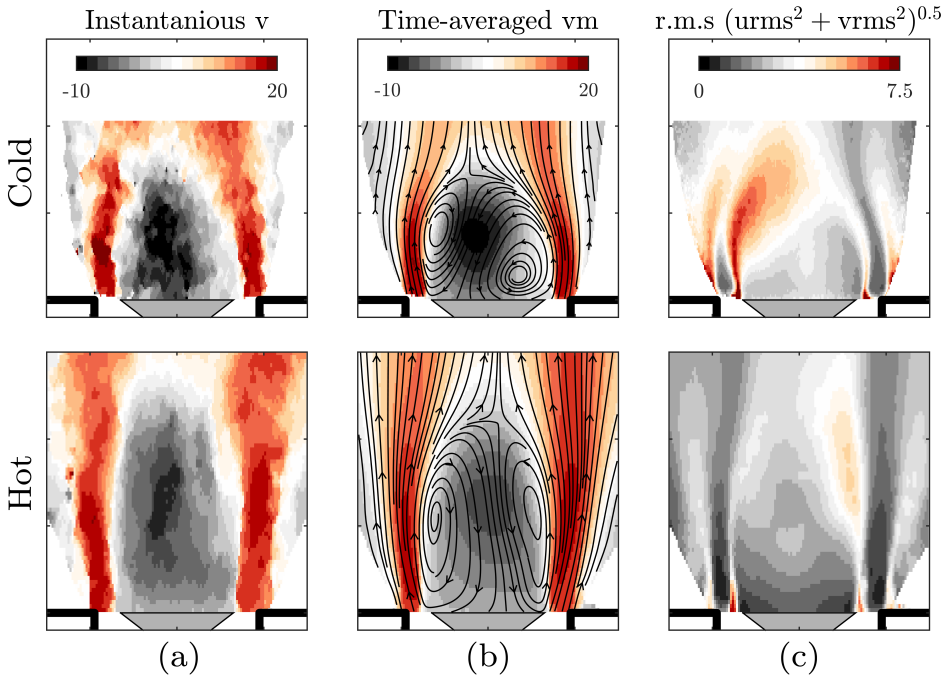

Figure 4: Fields of velocity fields from PIV. (a) Instantanious snapshot of v. (b) Time-averaged um. (c) r.m.s. fluctuation urms.

where the hierarchical structure of the data is opened in a file explorer. Hence, the data can easily be visualized by clicking through the folders and pressing "Plot Data".

The data is first organized into two main groups

1. **Flow:** Quantities related to the flow fields. These are further divided into Cold and Hot subgroups containing flow field data obtained for the non-reactive and reactive flows.

2. **Flame:** Quantities related to the flame. These are further divided into subgroups with data obtained from OH-Chemiluminecence and intensity obtained from OH-PLIF.

2.1. Flow fields

Time series data of the two velocity components (u, v) in the (x, y) directions were measured using planar high-speed PIV in the $x - y$ plane. For the non-reactive and reactive flows, the gas was seeded with oil and titanium dioxide respectively. The seeding particles were mixed in using a Laskin nozzle. The spatial resolution of the camera was ≈ 20 px/mm, and the displacement fields were processed using a multi-pass cross-correlation algorithm with an adaptive window search. The final size of the interrogation windows was 20-40 px^2 with 75% overlap.

The data fields contain

- The Cartesian coordinates x and y in (mm). These are stored as 2D (n_x, n_y) arrays, where n_x and n_y are the number of points in the x and y directions respectively.

- Time-series of instantaneous velocity fields u and v in (m/s). These are stored as 3D (n_x, n_y, n_t) arrays. The sampling rate used for the cold flow was 1 kHz. For the hot flow case 10 kHz was used.

- The time average velocity components um and vm in (m/s). These are stored as 2D (n_x, n_y) arrays.
- The r.m.s. fluctuations of the two velocity components urms and vrms in (m/s). These are stored as 2D (n_x, n_y) arrays.

A sample of the flow fields are shown in figure 4. From left to right (a) instantaneous, (b) time-averaged, and (c) r.m.s. fluctuations are shown respectively. The top row shows the cold flow case and the bottom row shows the reacting flow.

2.2. OH-Chemiluminecence

OH-Chemiluminecence was obtained with the camera fitted to a LaVision High-Speed IRO X intensifier, a 100mm Cerco UV lens, and a bandpass filter (310 ± 10nm). The spatial resolution of the camera was 11.33 px/mm. The camera intensities were normalized such that the integrated value of the time averaged image qm corresponds to the thermal power, i.e.

$$\int_A \mathrm{qm} dA = \mathrm{P} = 3.5\,\mathrm{kW}, \tag{4}$$

where a $dA = dxdy$ and A is the camera view. The data fields contain.

- The Cartesian coordinates x and y in (mm).
- The instantaneous HRR q integrated along the line of sight scaled in W/mm^2.
- The time averaged HRR qm integrated along the line of sight scaled in W/mm^2.
- The r.m.s. fluctuations of HRR $qrms$ integrated along the line of sight scaled in W/mm^2.
- The time averaged HRR in the $x-y$ plane qAm obtained through Abel deconvolution scaled in W/mm^3.
- R.m.s. fluctuations in HRR in the $x-y$ plane qArms obtained through Abel deconvolution scaled in W/mm^3.

The planar distribution qAm abd qArms were obtained by evaluating the Abel transform

$$\mathrm{qAm}(r, y) = -\frac{1}{\pi} \int_r^\infty \frac{\mathrm{dqm}(x, y)}{\mathrm{d}x} \frac{\mathrm{d}x}{\sqrt{x^2 - r^2}}, \tag{5}$$

using a 3pt-Abel deconvolution method. This operation transforms x into radial coordinates r and is done for the left and right sides of the flame separately.

A sample of the HRR fields are shown in figure 5. The three first fields from left to right (a-c) correspond to the instantaneous, time-averaged, and r.m.s. fluctuations of the line of sight integrated heat release rate. The two next panels (d and e) correspond to the time-averaged and r.m.s. fluctuations of the planar HRR.

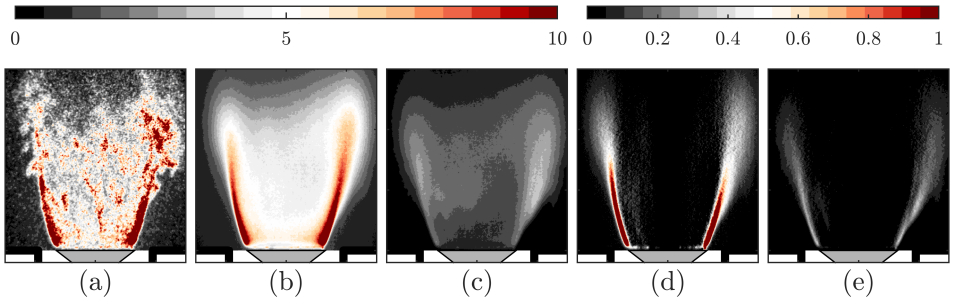

Figure 5: Fields of HRR from OH-chemiluminescence. (a) Instantanious snapshot q. (b) time-averaged qm. (c) r.m.s. fluctuation qrms. (d) time-averaged planar distribution qAm. (e) planar r.m.s. fluctuations qArms.

2.3. OH-PLIF

OH-PLIF was obtained in the centre $x-y$ plane. An Edgewave IS400-2-L nd:YAG (532 nm) laser was used to pump a Sirah Credo-Dye-N laser providing an output beam with a wavelength tuned to match the intensity peak of the OH-radicals at 283.569 nm. The intensifier gate time was reduced to 80 ns to capture only the signal excited by the laser proving a planar signal of the OH-concentration. Otherwise, the same camera setup as the one used for OH-chemiluminescence was used. A laser sheet correction is applied to the raw images to correct for intensity variations along the y direction due to the non uniform beam profile

$$\mathrm{I} = \mathrm{I}/L_s. \tag{6}$$

The function $L_s(y)$ is the time average laser sheet intensity obtained without the flame present. To account for shot-to-shot intensity variations in the laser output energy, the intensity of each image is corrected in the following way. First, each instantaneous image is integrated over space providing a time series of the global intensity variation

$$\mathrm{I}_{\mathrm{norm}}(t) = \int_A \mathrm{I}\mathrm{d}A. \tag{7}$$

The instantaneous images are then corrected by

$$\mathrm{I} = \mathrm{I}/(\mathrm{I}_{\mathrm{norm}}/\bar{\mathrm{I}}_{\mathrm{norm}}), \tag{8}$$

where the correction term reduces the intensity by the fluctuations around the mean of the integrated signal. This assumes that the integrated value of OH is quasi-steady.

The corresponding data fields contain

- The Cartesian coordinates x and y in (mm).
- The corrected instantaneous OH-PLIF signal I in arbitrary units.
- The time-averaged OH-PLIF signal Im in arbitrary units.
- The r.m.s. fluctuations of the OH-PLIF signal Irms in arbitrary units.

A sample of the OH-PLIF fields are shown in figure 6. From left to right the fields correspond to (a) the instantaneous, (b) time-averaged, and (c) r.m.s. fluctuations of the OH-PLIF intensity signal.

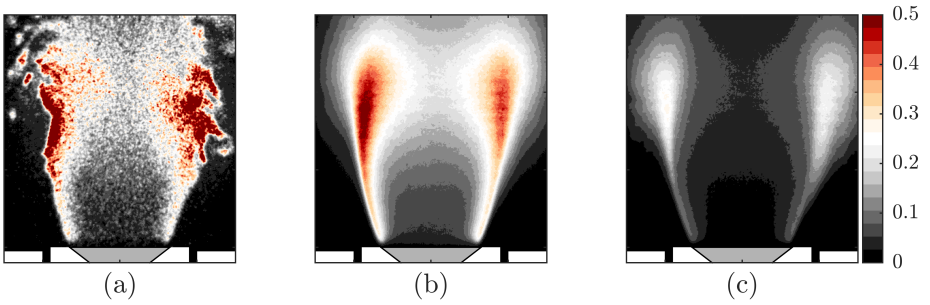

Figure 6: Fields of OH-PLIF intensity. (a) Instantaneous snapshot I. (b) time-averaged Im. (c) r.m.s. fluctuations Irms.

References

[1] E. Æsøy, J. G. Aguilar, S. Wiseman, M. R. Bothien, N. A. Worth, J. R. Dawson, Scaling and prediction of transfer functions in lean premixed h2/ch4-flames, Combustion and Flame 215 (2020) 269–282.

[2] E. Æsøy, J. G. Aguilar, M. R. Bothien, N. A. Worth, J. R. Dawson, Acoustic-convective interference in transfer functions of methane/hydrogen and pure hydrogen flames, Journal of Engineering for Gas Turbines and Power 143 (2021).

[3] E. Æsøy, H. T. Nygård, N. A. Worth, J. R. Dawson, Tailoring the gain and phase of the flame transfer function through targeted convective-acoustic interference, Combustion and Flame 236 (2022) 111813.

[4] E. Æsøy, T. Indlekofer, F. Gant, A. Cuquel, M. R. Bothien, J. R. Dawson, The effect of hydrogen enrichment, flame-flame interaction, confinement, and asymmetry on the acoustic response of a model can combustor, Combustion and Flame 242 (2022) 112176.

[5] E. Æsøy, The Effect of Hydrogen Enrichment on the Thermoacoustic Behaviour of Lean Premixed Flames, Ph.D. thesis, 2022.

[6] J. G. Aguilar, E. Æsøy, J. R. Dawson, The influence of hydrogen on the stability of a perfectly premixed combustor, Combustion and Flame 245 (2022) 112323.

[7] E. Æsøy, G. K. Jankee, S. Yadala, N. A. Worth, J. R. Dawson, Suppression of self-excited thermoacoustic instabilities by convective-acoustic interference, Proceedings of the Combustion Institute (2022).

[8] S. Wiseman, M. Rieth, A. Gruber, J. R. Dawson, J. H. Chen, A comparison of the blow-out behavior of turbulent premixed ammonia/hydrogen/nitrogen-air and methane–air flames, Proceedings of the Combustion Institute 38 (2021) 2869–2876.